C. Tsatsoulis · R. Kwok

Analysis of SAR Data of the Polar Oceans

Recent Advances

Springer

Professor Dr. Costas Tsatsoulis
The University of Kansas
Department of Electrical Engineering
and Computer Science
Snow Hall
Lawrence, Kansas 66045-2228
USA

Dr. Ronald Kwok
Jet Propulsion Laboratory
California Institute of Technology
4800 Oak Grove Drive
Pasadena, California 91109-8099
USA

ISBN 3-540-62802-9 Springer-Verlag Berlin Heidelberg New York

Library of Congress Cataloging-in-Publication Data
Tsatsoulis, C. (Costas), 1962-
Analysis of SAR data of the polar oceans : recent advances / C. Tsatsoulis, R. Kwok.
p. cm. Includes bibliographical references and index.
ISBN 3-540-62802-9 (hardcover)
1. Sea ice--Polar regions--Remote sensing. 2. Synthetic aperture radar.
I. Kwok, R. (Ronald), 1955- . II. Title.
GB2595.T73 1998 551.34'3'0911--dc21 97-37831

Printed in Germany

Cover Design: E. Kirchner, Springer-Verlag, Heidelberg
Production: ProduServ GmbH Verlagsservice, Berlin
Typesetting: MEDIO Innovative Medien Service GmbH, Berlin
SPIN: 10534645 32/3020-5 4 3 2 1 0 - Printed on acid -free paper

Mapping the Progression of Melt Onset and Freeze-Up on Arctic Sea Ice Using SAR and Scatterometry

D.P. Winebrenner, D.G. Long, B. Holt

Contents

7.1 Introduction

The annual changes of seasons, their timing, and their variations from place to place reflect and drive many processes of geophysical import, as well as a wide range of human activities. In remote parts of the world, including the Arctic, knowledge and understanding of annual and interannual cycles has been limited by a paucity of observational data. Satellite observations promise to illuminate many relationships and underpin new theoretical understanding. Seasonal transitions on Arctic sea ice are especially germane to studies of global climate and links between high latitude and global geophysical processes.

For example, Scharfen et al. (1987) have reported evidence, based largely on satellite observations, that the date when Arctic sea ice begins to melt is related to the areal extent of sea ice remaining in late summer, which significantly affects global albedo (Ebert and Curry 1993). It is widely thought that the length of the melt season, i.e., the number of days between spring melt onset and autumn freeze-up, strongly influences the sea ice mass balance budget (Maykut and Untersteiner 1971; Ebert and Curry 1993), which in turn influences global ocean circulation (Aagaard and Carmack 1994). Parkinson (1992), using satellite passive microwave data, has noted significant geographical and interannual variability in melt season length. Carsey (1985) observed that Arctic sea ice backscatter seemed to respond to the end of the melt season, i.e., the autumn freeze-up, and that the progression of this event northward could be traced in the record.

In all cases, however, the relevant satellite records are short, their analysis is to some degree uncertain because of limited understanding of the physics underlying the observations, and the necessary analysis was highly labor intensive and therefore slow and limited. To realize the promise in satellite remote sensing, we must learn how to

Analysis of SAR Data of the Polar Oceans
Edited by C. Tsatsoulis and R. Kwok

onset signature change is clear. For freeze-up, Winebrenner et al. (1996) combined a wide area SAR study in the Beaufort and Chukchi Seas with a buoy temperature/SAR study in the Beaufort and concluded that temporally erratic but generally low summer backscattering cross sections stabilize at winter multiyear ice values (roughly -9 dB) within 7 days of continuously subfreezing air temperatures. Schwartz et al. (1994) observed spring and autumn transitions in the Beaufort and Chukchi Seas, but compared with analyzed temperature fields based primarily on shore-based data, and reached similar conclusions.

In an effort to reap the advantages of SAR while mitigating the costs, Winebrenner et al. (1994; 1996) proposed and demonstrated machine-automatable algorithms for retrospective estimation of melt onset and freeze-up dates within geographical cells using ERS-1 SAR imagery. This approach utilizes many low-resolution (100-m) SAR images but immediately reduces the information volume to time series of backscattering cross section histograms, one for each geographic cell. This avoids any need to monitor backscattering cross section histories for individual ice floes.

More or less simultaneously with these developments, several investigators found that characteristic seasonal backscattering changes could also be identified for several terrestrial targets in addition to sea ice. An illustrative, rather than exhaustive, list of examples includes the following. Smith et al. (1997) found that ERS-1 SAR backscatter observations of alpine glaciers show clearly the onset and progression of spring melt. On the Greenland ice sheet, Drinkwater and Long (1994) found that 14.6 GHz backscattering observed using the Seasat wind scatterometer not only delineated snow zones in winter but showed clearly the progression and extent of the melt season at all altitudes. Early et al. (1994) found evidence of temporal variation in snow facie boundaries between 1978 and 1991 by comparing scatterometer observations from ERS-1 with those from Seasat. Wismann et al. (1996) found continuous temporal variation from 1991 to 1995 in 5.3-GHz ERS-1 scatterometer observations of Greenland, and found valuable seasonal information in scatterometer observations of Siberian tundra, the Sahel, and tropical and boreal forests as well. Thus, the observations of seasonal transitions on sea ice may be seen within a wider geophysical and remote sensing context, and methods developed in connection with sea ice may prove useful in developing automated processing methods for other geophysical targets and variables.

In this chapter, we begin with a review of the methods and results of Winebrenner et al. (1994, 1996) for automatable mapping of seasonal transition dates and melt season length on Arctic sea ice. This review includes neither new data nor results, but we focus particularly on the problems and essential features of machine automation that contribute to a useful geophysical data product. In the following section, we present new results based on Seasat wind scatterometer observations and the resolution enhancement algorithm of Long et al. (1993) for the freeze-up period in the Beaufort and Chukchi Seas during 1978. We briefly compare these results with those obtained by Drinkwater et al. (1994) for seasonal transitions on Antarctic sea ice. The observations clearly show the observability of freeze-up and its temporal progression in 14.6-GHz observations, as well as the applicability of Long's resolution enhancement method to moving targets such as sea ice during a period of temporal change. Thus it appears that scatterometry data may usefully serve to set the context for, augment, or in some cases substitute for SAR observations even for targets such as sea ice that vary strongly on small horizontal scales. Insight gained in the development of methods for SAR and scat-

interpret the observations in a quantitative physical sense, and we must implement the interpretative operations on machines that can keep pace with the torrent of raw data that satellites provide.

The fine spatial resolution provided by synthetic aperture radar (SAR) can aid quantitative, physical interpretation of observations in cases where, as in the case of sea ice, the geophysical medium of interest varies greatly on horizontal scales of tens of meters to hundreds of kilometers. Spatial resolution allows one to focus attention on sea ice of a particular type (e.g., leads, thick first-year ice, multiyear ice, ridges, etc.) for which a theoretical understanding of signatures may be available. The use of fine spatial resolution avoids mixing signatures of various ice types into an average which cannot, in general, be uniquely unmixed, or which can be unmixed only by a laborious analysis using ancillary information.

There are, however, prices for to be paid the advantages of SAR. One of these has been a limitation in swath width and temporal coverage; various design and information throughput constraints limit the width of the SAR image strip and the interval between revisits of a given geophysical target. Thus what is gained in interpretability may be lost in lack of context over the largest relevant spatial scales or shortest time scales. There is, in addition, a danger of drowning in data while trying to extract a relatively small volume of information. This is the background against which recent work to utilize SAR to observe seasonal transitions on Arctic sea ice should be viewed.

A SAR image of sea ice is essentially a snapshot of the spatially varying backscattering cross section of the ice. Ground-based and airborne measurements (Onstott et al. 1987; Livingstone et al. 1987; Barber et al. 1992; Carlstrom and Ulander 1993; Beaven and Gogineni 1994) show that like-polarized backscattering cross sections of sea ice, at frequencies from 5 GHz upward, change at the beginning and again at the end of the melt season. In the case of autumn freeze-up, the measurements of Carlstrom and Ulander (1993) and Beaven and Gogineni (1994) provided fine temporal resolution of the 6- to 10-dB change, with continual observations of the same ice samples. Their simple but convincing modeling indicated the physical cause of the change to be an increase in volume scattering from air bubbles in the upper 10–20 cm of ice as dielectrically lossy liquid water froze into low-loss, relatively fresh ice. The timing of the freeze-up signature change followed within a week the onset of sustained air temperatures below freezing. In the case of melt onset, fine temporal resolution observations of individual ice floes were rare or uncalibrated, but the observations did indicate a decrease for multiyear ice of roughly 7–12 dB between periods before and after the beginning of melting. Temporal changes in first-year ice signatures are evidently smaller and more subtle (Barber et al. 1992).

Winebrenner et al. (1994) used temperature records from drifting buoys and nearly coincident SAR imagery from the first European Remote Sensing (ERS-1) satellite to show that sharp, 9-dB drops in multiyear ice backscattering cross sections (at 5.3 GHz, VV-polarization) coincided, to within 2–4 days, with rises in air temperature to 0°C at locations in the Beaufort Sea between 72°N and 82°N during June 1992. Theoretical analysis by these authors showed that the cross-section drop is due solely to the appearance of liquid water in the snow overlying the multiyear ice. Essentially, the strong 5.3-GHz backscattering from the bubbly upper layer of multiyear ice dominates the SAR return while the snow is dry, but moist snow strongly attenuates illumination of, and scattering from, the bubbly layer. Thus the physical event corresponding to the melt

onset signature change is clear. For freeze-up, Winebrenner et al. (1996) combined a wide area SAR study in the Beaufort and Chukchi Seas with a buoy temperature/SAR study in the Beaufort and concluded that temporally erratic but generally low summer backscattering cross sections stabilize at winter multiyear ice values (roughly -9 dB) within 7 days of continuously subfreezing air temperatures. Schwartz et al. (1994) observed spring and autumn transitions in the Beaufort and Chukchi Seas, but compared with analyzed temperature fields based primarily on shore-based data, and reached similar conclusions.

In an effort to reap the advantages of SAR while mitigating the costs, Winebrenner et al. (1994; 1996) proposed and demonstrated machine-automatable algorithms for retrospective estimation of melt onset and freeze-up dates within geographical cells using ERS-1 SAR imagery. This approach utilizes many low-resolution (100-m) SAR images but immediately reduces the information volume to time series of backscattering cross section histograms, one for each geographic cell. This avoids any need to monitor backscattering cross section histories for individual ice floes.

More or less simultaneously with these developments, several investigators found that characteristic seasonal backscattering changes could also be identified for several terrestrial targets in addition to sea ice. An illustrative, rather than exhaustive, list of examples includes the following. Smith et al. (1997) found that ERS-1 SAR backscatter observations of alpine glaciers show clearly the onset and progression of spring melt. On the Greenland ice sheet, Drinkwater and Long (1994) found that 14.6 GHz backscattering observed using the Seasat wind scatterometer not only delineated snow zones in winter but showed clearly the progression and extent of the melt season at all altitudes. Early et al. (1994) found evidence of temporal variation in snow facie boundaries between 1978 and 1991 by comparing scatterometer observations from ERS-1 with those from Seasat. Wismann et al. (1996) found continuous temporal variation from 1991 to 1995 in 5.3-GHz ERS-1 scatterometer observations of Greenland, and found valuable seasonal information in scatterometer observations of Siberian tundra, the Sahel, and tropical and boreal forests as well. Thus, the observations of seasonal transitions on sea ice may be seen within a wider geophysical and remote sensing context, and methods developed in connection with sea ice may prove useful in developing automated processing methods for other geophysical targets and variables.

In this chapter, we begin with a review of the methods and results of Winebrenner et al. (1994, 1996) for automatable mapping of seasonal transition dates and melt season length on Arctic sea ice. This review includes neither new data nor results, but we focus particularly on the problems and essential features of machine automation that contribute to a useful geophysical data product. In the following section, we present new results based on Seasat wind scatterometer observations and the resolution enhancement algorithm of Long et al. (1993) for the freeze-up period in the Beaufort and Chukchi Seas during 1978. We briefly compare these results with those obtained by Drinkwater et al. (1994) for seasonal transitions on Antarctic sea ice. The observations clearly show the observability of freeze-up and its temporal progression in 14.6-GHz observations, as well as the applicability of Long's resolution enhancement method to moving targets such as sea ice during a period of temporal change. Thus it appears that scatterometry data may usefully serve to set the context for, augment, or in some cases substitute for SAR observations even for targets such as sea ice that vary strongly on small horizontal scales. Insight gained in the development of methods for SAR and scat-

terometry appear to be mutually complementary. We conclude with a discussion of what we believe to be the most important issues to be addressed in future work, both to extend methods and to begin to address important geophysical questions using automated methods.

7.2 Synopsis of Transition Date Mapping Using the ERS-1 SAR

The essential phenomena on which automatable mapping of melt onset and freeze-up relies are, respectively, the striking drop in multiyear ice 5.3-GHz backscattering cross sections in spring, and the restabilization of those cross sections at relatively high winter values in the autumn.

As summarized in the Introduction, and discussed in detail by Winebrenner et al. (1994), the springtime drop in cross sections coincides with the rise of local air temperatures to 0°C to within 2–4 days. This is shown graphically in Fig. 1 for a case with a particularly reliable temperature record. Figure 2 shows the visible manifestation of the phenomenon in ERS-1 SAR imagery. The physical cause of the change is the appearance of liquid water in the snowcover on the ice. Volumetric snow moisture of as little

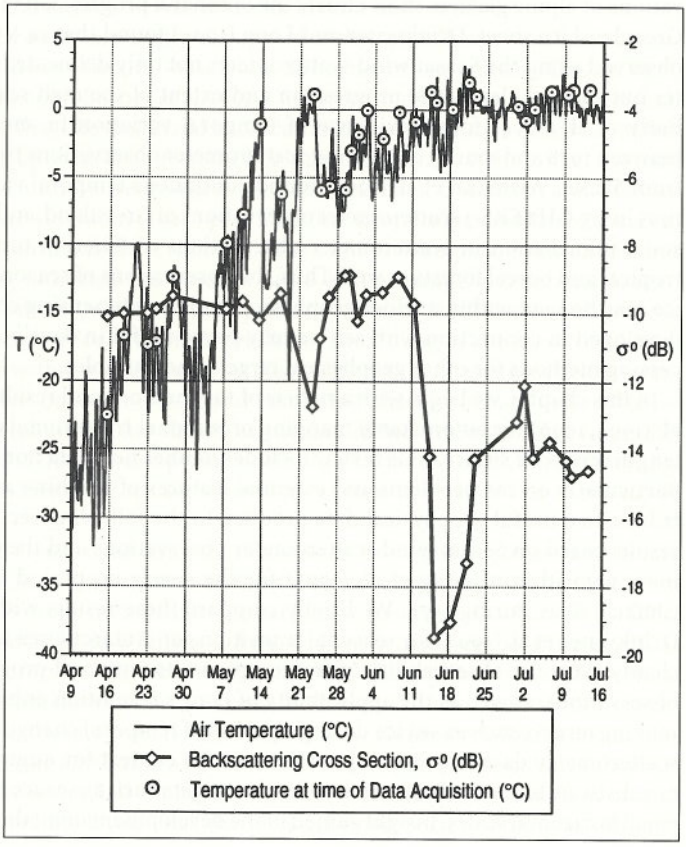

Fig. 1. Near-surface air temperature from a drifting buoy in the Beaufort Sea, and the 5.3-GHz, VV-polarized backscattering cross-section of multiyear ice near the buoy as observed using the ERS-1 SAR, during the period mid-April to July, 1992. The *circled dots* on the temperature record denote the temperatures at the time of SAR data acquisition

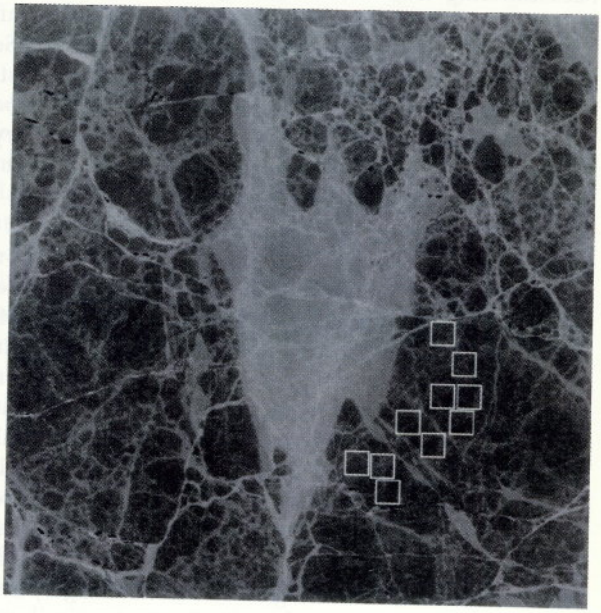

Fig. 2. **a** ERS-1 SAR image of a representative ice region on June 2, 1992, near the buoy that provided the data in Fig. 1. Temperatures were still well below freezing. **b** A similar image of the same ice scene on 15 June 1992, just after the onset of melt. Equal gray levels in separate images connote equal backscattering cross-sections. The *white rectangular regions* define sampling boxes used in previous signature-change study. (Copyright ESA 1992)

as 2% renders previously (dry) microwave-transparent snow quite lossy; thus illumination of the strongly scattering bubbly upper layer of multiyear ice is reduced, and scattered returns are attenuated by their passage through the snow. In the earliest stage of melt onset, this is all the microwave physics that matters. The fact that the strong scatterer beneath the snow happens to be a bubbly layer is not essential – any strong backscatterer would produce similar phenomenology because the shielding by newly wet snow is the source of the change. The difficulty in sensing melt onset on first-year ice at 5.3-GHz is the weakness of winter first-year ice backscattering. The drop in backscattering due to shielding of an already weak scatterer is difficult to observe, especially from space. (Note, however, that these comments apply only to the earliest stage of melt onset; scattering from both first- and multiyear ice increases to high levels within roughly 2 weeks of melt onset, probably because the snow surface becomes water-logged and rough. Utilization of the information contained in this latter signature variation is a topic of current research in several groups.) Spaceborne observation of melt onset on first-year ice might well be facilitated by observation at a wavelength where winter first-year ice cross sections are higher. We return to this point in the next section.

Two considerations directly influence the design of machine automatable algorithms for melt onset detection. First, the drop in backscattering cross sections varies slightly between multiyear ice floes, but is large – typically 7–10 decibels – for virtually every individual floe (Winebrenner et al. 1994). Thus it is not necessary to monitor the backscattering cross-section history of individual multiyear floes to observe melt onset; it is only necessary to derive from imagery information on the temporal backscattering evolution of typical multiyear ice pixels. Second, near-surface air temperatures over Arctic sea ice are highly correlated over distances on the order of at least 100 km (Rigor and Muñoz, "Statistics of Surface Air Temperature Observed in the Arctic", manuscript in preparation, 1996). Thus it is necessary only to sample Lagrangian regions of size on the order of 100 km with SAR imagery to produce a map of melt onset dates with useful spatial resolution.

For regions covered predominantly by multiyear ice at the time of melt onset, these considerations suggest a simple algorithm. Divide the region of interest into fixed (Eulerian) grid cells of the minimum dimension consistent with high temporal resolution of sampling with SAR imagery around the time of melt onset (preferable sizes will be on the order of 100 km or less). Assign each SAR image to a grid cell, and compute for each image a histogram of pixels with backscattering cross-sections in narrow ranges. Because the most probable surface cover is multiyear ice (in the selected regions), simply track the backscattering cross section value of the peak (mode) of the histogram through time; the time series of such peak values is a reasonable proxy for multiyear ice backscattering cross sections under the stated conditions. Set a threshold such that when the proxy for multiyear ice cross-sections crosses the threshold from above, melt onset is inferred to have taken place within the entire cell. This algorithm was automated and run using all ERS-1 SAR imagery over the Beaufort Sea collected by the Alaska SAR Facility (ASF) during spring 1992, with the result shown in Fig. 3. This particular map used cells of 200 km on a side on the grid defined for Special Sensor Microwave/Imager (SSM/I) brightness temperatures. The algorithm required operator intervention in one cell, denoted with a numeral 2 in the map, where an early "false start" to melt onset occurred – backscattering dropped briefly in late May but then

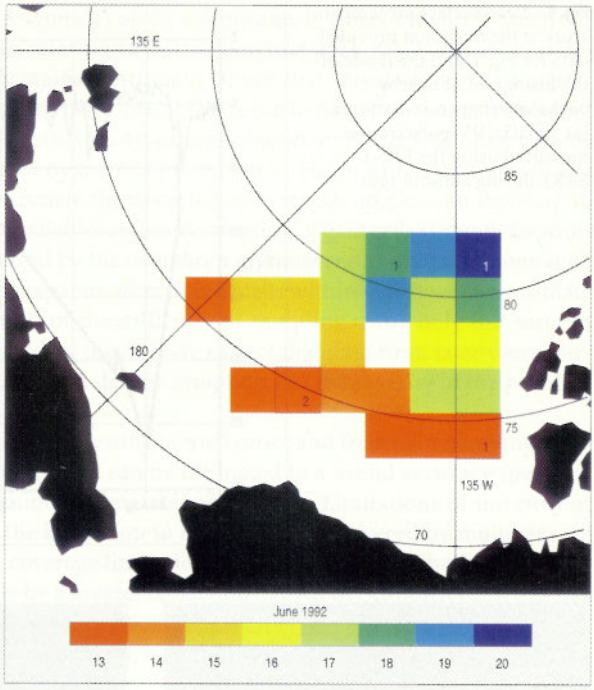

Fig. 3. Map of the dates of melt onset estimated from ERS-1 SAR data and the algorithm of Winebrenner et al. (1994), for the spring of 1992 in the Beaufort Sea. The cells are square and measure 200 km on a side; they coincide with groups of cells on the SSM/I grid. *Unshaded cells* indicate a lack of sufficient data or that the area contains less than 50% multiyear ice

quickly returned to winter levels until mid-June, when backscattering began a typical summer progression. The inferred melt onset dates shown in Fig. 3 agree with independent estimates of those dates from buoy data, to within 4 days (Winebrenner et al. 1994). In cells where temperatures repeatedly reach 0 °C and refreeze during spring, the algorithm will pick the first date of melting as the melt onset date. The largest single source of uncertainty in satellite-derived melt onset dates in the study of Winebrenner et al. (1994) was the temporal lag between SAR images sampling each grid cell; thus there is the prospect of reducing such uncertainty in future studies.

The fundamental phenomenology underlying mapping of autumn freeze-up, i.e., the transition from temporally erratic, sometimes high but often low backscattering to high, stable backscattering, is illustrated in Fig. 4, and its visual manifestation in SAR imagery is shown in Fig. 5. The physics of the transition is more difficult to model in a precise, quantitative way, but there is little doubt that the freezing of liquid water and consequent rise in backscattering from the bubbly upper layer of refreezing ice is the primary physical cause of changes in backscattering from ice floes (Carlstrom and Ulander 1993; Beaven and Gogineni 1994). In the case of freeze-up, however, areally averaged backscattering often displays a peculiar overshoot phenomenon, in which cross sections initially increase to 1–2 dB above winter values around the time of the decrease in temperatures from near to below freezing (for the final time in the year). The cross sections then gradually settle back to typical winter multiyear ice values within 7–10 days.

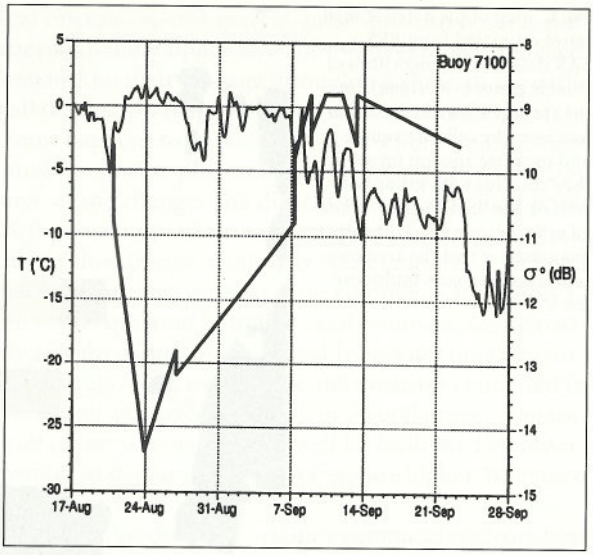

Fig. 4. Near-surface air temperature at the buoy that provided data for Fig. 1, and the mode of the histogram of nearby backscattering cross-sections (at 5.3 GHz, VV-polarization, measured using the ERS-1 SAR), during autumn 1992

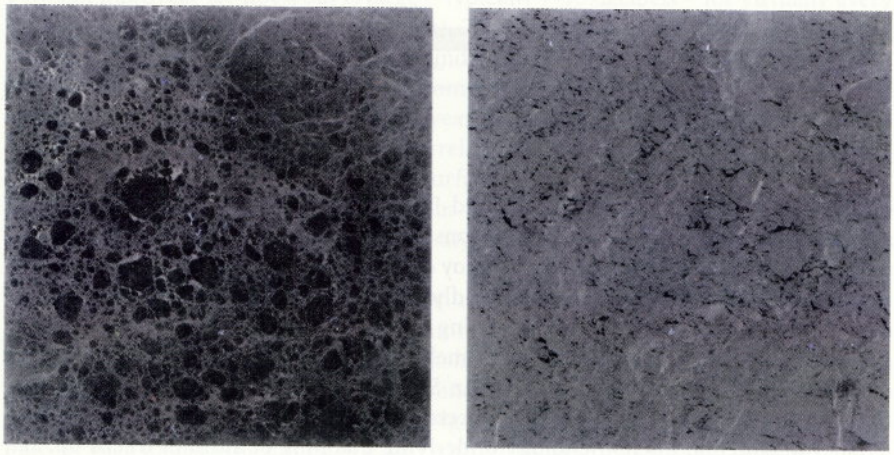

Fig. 5. **a** ERS-1 SAR image of a representative ice region on September 6, 1992, near the temperature-reporting buoy of Figs. 1 and 4. Temperatures were near freezing at the time of image acquisition. **b** Similar image data from another region near the same buoy on September 8, 1992, after temperatures had dropped below freezing. Equal gray levels in separate images connote equal backscattering cross sections. (Copyright ESA 1992)

This observation led to the following automatable algorithm for retrospective estimation of freeze-up dates. Using the method of SAR image sampling on the fixed grid from the melt onset algorithm, and limiting consideration to regions in which the areal coverage by summer ice is greater than 50% at the end of the summer, consider time series of histograms of backscattering cross sections from the images sampling each

grid cell. Again, track the peaks (mode) of the histograms in time (which, by construction, indicate typical ice backscattering values). When that peak value crosses a predetermined threshold, X, and remains continually above that threshold for a predetermined number of days, N, estimate the time of freeze-up to have been some number of days, M, prior to the threshold crossing. An example based on ERS-1 SAR observations of the Beaufort Sea (as acquired by the ASF) is shown in Fig. 6, with $X = -10.5$ dB, $N = 10$ days, and $M = 0$ days. We estimate the uncertainty in freeze-up dates on this map to be ±4 days, due largely to the available temporal sampling of grid cells (though an additional uncertainty may be caused by the overshoot phenomenon) (Winebrenner et al. 1996). This, as well as the rather sparse collection of cells within which we can estimate freeze-up dates, is an indication of the difficulty of sampling using only the autumn 1992 ERS-1 SAR images collected by the ASF. We expect that data from later years during the life of the satellite can provide denser sampling, but the severity of the problem is noteworthy.

Nonetheless, the construction and testing of melt onset and freeze-up mapping algorithms shows that melt season lengths can be estimated to a useful accuracy (perhaps 5%) using SAR data and machine automatable algorithms. Limitations of the current data and algorithms include the limitation to regions largely covered by multiyear ice and the temporal and spatial coverage limitations of early SAR data. Though the latter problem may be solved simply by a greater collection of SAR or ScanSAR data, this has yet to be demonstrated (and in the case of ScanSAR introduces the complication of varying incidence angles). In the next section, we present observations that may point the way toward an easing of these limitations.

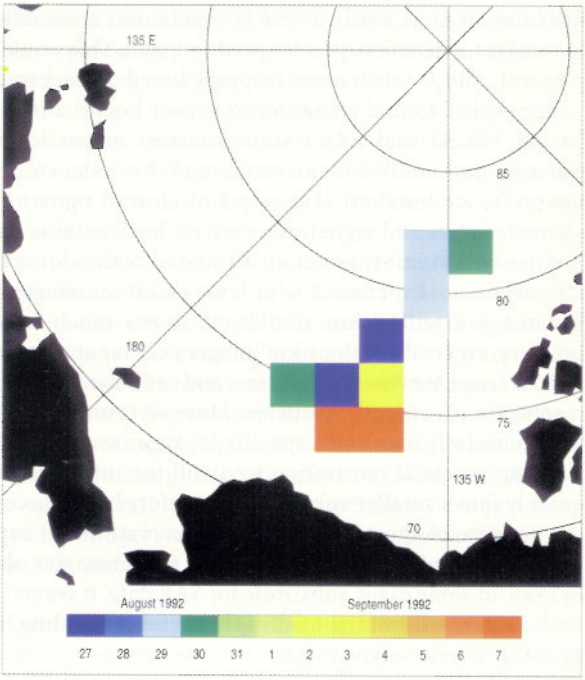

Fig. 6. Map of the dates of freeze-up estimated from ERS-1 SAR data and the algorithm of Winebrenner et al. (1996)

7.3
Enhanced-Resolution Scatterometer Observations of Freeze-Up

Spaceborne scatterometers are stable, well-calibrated instruments for measuring backscattering cross sections, albeit at spatial resolutions coarser than the scales of cross section (and geophysical) variability inherent in some geophysical targets. (For a discussion of relevant operational details of spaceborne scatterometry, including the matter of normalization to a standard incidence angle, see Long et al. 1993).

We are motivated to investigate the utility of scatterometers for observing seasonal transitions on sea ice for at least two reasons. The first is a prospective advantage stemming from the shorter wavelength (higher frequency) at which many spaceborne scatterometers operate, relative to that of Radarsat or the ERS-1 and -2 SARs and scatterometers. At the frequency (5.3 GHz) of those latter instruments, backscattering from winter first-year sea is weak. Hence it is difficult to observe the melt onset transition on first-year ice and to automate data interpretation in areas covered mostly by first-year ice (see the previous section). However, the operating frequency of the Seasat scatterometer was 14.6 GHz, and that of the new NASA scatterometer (NSCAT) is 14.0 GHz. Ground-based observations near those frequencies (Onstott 1992) indicate that winter backscattering from first-year ice is considerably higher than at 5.3 GHz (though the physical reason for this is not clear as of this writing). Dry snow would be expected, on theoretical and observational grounds to be slightly less transparent at the higher frequencies than at 5.3 GHz, but a given thickness of wet snow would be expected to be a more effective shield (Hallikainen and Winebrenner 1992). Therefore we would expect a much stronger drop in 13- to 15-GHz backscattering cross sections at melt onset than is observed at 5.3 GHz. This would make backscattering observations at the higher frequencies far more easily usable for melt onset observation in areas such as the Siberian shelves, where first-year ice predominates. This would significantly expand the geophysical utility of melt onset mapping based on backscattering.

The typical spatial resolutions of space borne scatterometers, however, and of the Seasat, NSCAT and ERS-1 scatterometers in particular, are nominally 50 km. As Carsey (1985) and Wismann et al. (1996) have shown, even this resolution is of some use on sea ice, but there is mixing and a loss of signature information because sea ice characteristics and signatures vary on horizontal scales as short as meters. This is not to say that information on all spatial scales down to meters is always useful for all purposes – experience with low-resolution imagery of sea ice indicates that sea ice imagery with 5-km resolution shows much more information than 50-km imagery, especially if the 5-km imagery comes at an acceptable price in terms of spatial coverage, temporal resolution, and radiometric fidelity. As we discuss below, such resolution is evidently available. Moreover, while the resolution of SAR provides a way to usefully focus on a specific ice type (see the previous section), there remains a strong practical motivation to distill the information in a high-resolution image quickly into a smaller volume. We therefore have a second motivation, in addition to the promise of shorter wavelength observations, to explore further the potential of enhanced-resolution scatterometry – scatterometer observations may complement or even, in some cases, substitute for SAR data. It seems likely that whatever is learned in this effort will contribute insight useful in building better automated SAR, as well as scatterometer, algorithms.

Long et al. (1994) have in fact begun this process using ERS-1 scatterometer data from the Weddell Sea and an adaptation of the resolution enhancement method of Long et al. (1993). Heuristically, Long's Scatterometer Image Reconstruction with Filtering (SIRF) operates by combining scatterometer observations from footprints whose backscatter values are correlated because of they share area in common. The aim is to reconstruct the underlying, fine-scale map of backscattering cross-section, given sufficient knowledge of the overlap geometries. In practice, the scatterometer observations are acquired over some time interval, during which the target could change; any such temporal variation is treated as "noise" in the algorithm. The SIRF algorithm is based on an iterative, multivariate modification of multiplicative algebraic reconstruction; the standard version of the latter is a special case of maximum-entropy reconstruction. In cases where footprint overlap is insufficient to completely determine all matrix elements in the estimation problem, a maximum-entropy-based assumption is used to specify those elements. This is, in effect, an assumption concerning the autocorrelation structure of the underlying backscattering map at subresolution scales (Jaynes 1982; see also pages 420–426 of Percival and Walden 1993), namely that the correlation is that of the most random, least predictable structure on those scales that is consistent with the observations at larger scales. The assumption is likely to be more accurate when noise is limited (Jaynes 1982). The result is a map of backscattering cross-section estimates on a finer grid than the original data, consistent with the assumptions on that underlying map and "noise" inherent in the method.

In the case of sea ice, ice motion and possible temporal changes limit the period of time over which observations of a given ice region may be accumulated, and therefore the fineness of the resulting grid of backscattering cross-sections relative to the original data resolution. In the case of the study of Long et al. (1994) in the Weddell Sea, this interval was 7 days and allowed enhancement from 50 km to 25 km. In the case of the Seasat scatterometer, differences in predelivery processing of the data allowed greater enhancement, to 9 km, while accumulating data over 8-day intervals.

From the preceding discussion, it is clear that high-frequency scatterometer observations of melt onset as well as freeze-up would be valuable. However the lifetime of the Seasat, together with the unavailability of NSCAT data as of this writing, limit our high-frequency observations for now to freeze-up during 1978. The promise of higher-frequency observations is strikingly evident, nevertheless, in the measurements we have. Figure 7 shows temperature, precipitation, and backscattering cross section time series from 1978, the former measured at Mould Bay in the Canadian Archipelago, the latter from a time series of resolution-enhanced, 14.6-GHz backscattering images based on data from the Seasat wind scatterometer. Because the location of the backscatter measurements is just west of the temperature measurement site, small temporal offsets between events in the temperature and backscatter records might be expected. Nonetheless, the highly variable backscattering characteristic of summer conditions quickly gives way to high, stable backscattering after September 15 (Julian day 258), giving a clear indication of freeze-up. Even rather short, minor melting events just prior to freeze-up seem to be reflected in the backscattering record. This appears to be consistent with the pattern seen in SAR studies at 5.3 GHz (see the previous section and Winebrenner et al. 1996).

Figure 8 shows a series of 22 wide-area images including the Alaskan coast and the Beaufort and Chukchi Seas, with a pixel spacing of 9 km. The series begins on July 8

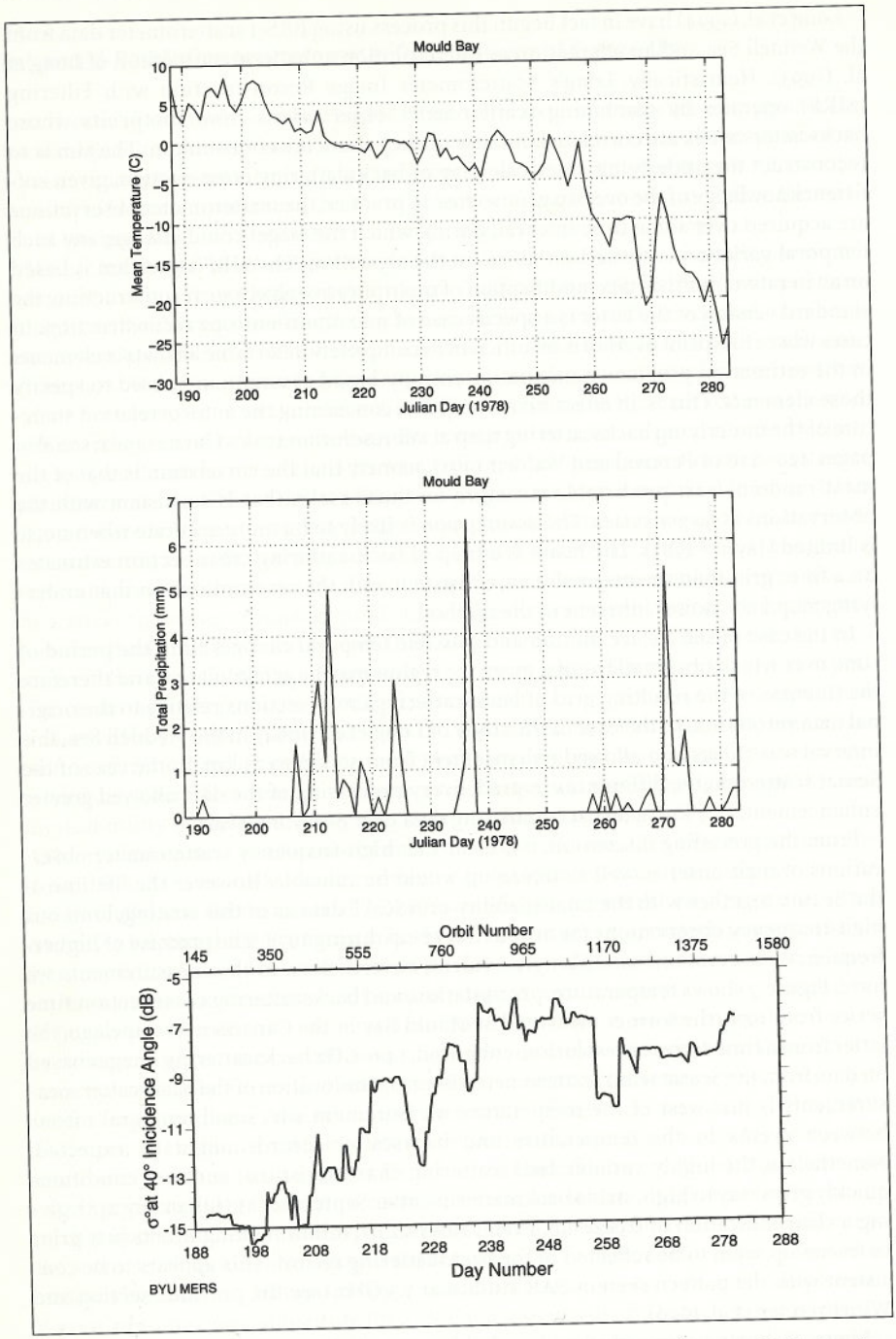

Fig. 7. a-c. Time series of a temperature and b precipitation at Mould Bay, and c 14.6-GHz backscattering from sea ice just to the west, as measured with the Seasat scatterometer, during autumn 1978

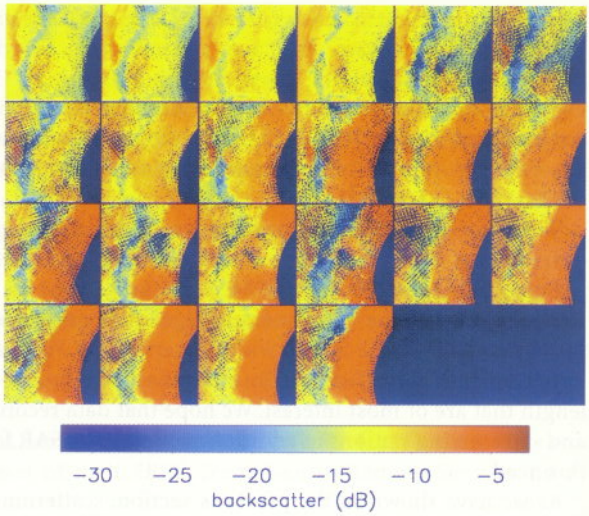

Fig. 8. A time series of 22 enhanced-resolution Seasat scatterometer images, each resulting from data accumulation of 8 days, at time intervals 4 days apart (data accumulations for adjacent images overlap by 4 days). The time series begins on July 8, 1978 and ends on October 8, 1978. Each image is presented in a polar stereographic projection with center coordinate 70°N, 225°E, and measures approximately 1468.5 km on its horizontal axis and 1530.8 km on its vertical axis. Pixel spacing is 8.9 km. The coast of Alaska is visible in most images as the relatively high backscatter region along the *left borde* *r*. Th on the right of each image is the region in which no data are available due to the limiting latitude of the Seasat orbit

(Julian day 189), and continues to October 7 (Julian day 280). The images are spaced 4 days apart; the 8-day data accumulation intervals for each pair of images overlap by 4 days. The north-to-south progression of stable, high backscattering marking freeze-up is very clear, at least for regions known independently to be covered in winter largely by multiyear ice. Note that freeze-up either has not occurred or is not so clearly visible in the area near the Alaskan coast at the end of the image series.

This response at 14.6 GHz in the Arctic stands in contrast to that observed with 5.3 GHz scatterometry in the Antarctic (Drinkwater et al. 1994). In the latter case, freeze-up is marked much more subtly by a slight decrease in backscattering at the reference incidence angle (40°), but the change in the gradient of backscattering with incidence angle is pronounced.

It is clear in any case that 14.6 GHz (or, almost equivalently, 14.0 GHz) backscattering and enhanced-resolution scatterometry of Arctic sea ice can provide freeze-up, and very likely melt onset, information. It is likely that such information can be obtained on first-year as well as multiyear Arctic sea ice using the higher frequencies. The wide geographic coverage of scatterometer data make them complementary, and perhaps in some cases a substitute for, SAR data. Moreover, the use of scatterometry involves observations at a number of incidence angles and referencing those observations to a common incidence angle (Long et al. 1993); experience in learning to use scatterometry data may therefore be highly valuable in learning to use wide-swath, multi-incidence angle (i.e., ScanSAR) data as well. Hence there is considerable motivation to expand attempts to automate seasonal transition date mapping on sea ice to include scatterometer and higher-frequency SAR observations.

7.4 Future Work

Clearly much work on, and involving, automated mapping of seasonal transitions on sea ice remains to be done as of this writing. Methods and observations to date are no more than prototypes; neither mature technology nor geophysically useful data sets yet exist.

We believe the single most pressing need, from both a geophysical and an algorithm-development standpoint, is for observational studies outside the popular Beaufort Sea region. There is evidence that SAR signatures of sea ice vary significantly across the Arctic basin, and the adjustment of algorithm parameters or entire algorithms may prove necessary in the face of wider observations. From a geophysical standpoint, it is Arctic-basin-scale variations in melt onset and freeze-up timing and melt season length that are of most interest. We hope that data records now available from ERS-1- and -2-receiving stations in addition to the Alaska SAR facility can be used to address this need.

As we have shown in the previous section, scatterometer data and backscattering observations at 13–15 GHz hold considerable promise for extending seasonal transition mapping. However, the physics of the relevant phenomenology, especially strong winter backscattering from first-year ice, is not well understood. We cannot say how broadly, in a geographical sense, higher frequency data may be useful without a better understanding of why the phenomenon arises, and therefore when, if ever, it is likely not to arise. A physical understanding of backscattering also aids the multiple-incidence angle processing necessary in constructing enhanced resolution scatterometer imagery and ScanSAR imagery (e.g., RADARSAT).

Finally, from a purely geophysical standpoint, seasonal transition dates have been mapped so far, by whatever means, for very few years in the Arctic. Progress on questions about the role of the Arctic in global climate and possible climate change cannot be addressed without decadal and multidecadal time series. We therefore hope that the next few years will bring the publication and availability of such time series. We believe that with such availability, the role of automated interpretation of satellite observations investigating polar geophysical questions will be greatly strengthened.

References

Aagaard K, Carmack EC (1994) The Arctic Ocean and climate: a perspective. AGU Geophys Monogr 85

Barber DG, LeDrew EF, Flett DG, Shokr M, Falkingham J (1992) Seasonal and diurnal variations in SAR signatures of landfast sea ice. IEEE Trans Geosci Remote Sens 30, no 3: 638–642

Beaven SG, Gogineni SP (1994) Shipborne radar backscatter measurements from Arctic sea ice during the fall freeze-up. Remote Sens Rev 9: 3–25

Carlstrom A, Ulander LMH (1993) C-band backscatter signatures of old sea ice in the central Arctic during freeze-up. IEEE Trans Geosci Remote Sens 31, no 4: 819–829

Carsey F (1985) Summer Arctic sea ice character from satellite microwave data. J Geophys Res 90, no C3: 5015–5034

Drinkwater MR, Early DS, Long DG (1994) ERS-1 investigations of Southern Ocean sea ice geophysics using combined scatterometer and SAR images. Proc Int Geosci Remote Sens Symp IGARSS '94, August 8–12, Pasadena, California, pp 165–167

Early DS, Long DG, Drinkwater MR (1994) Comparison of enhanced resolution images of Greenland from ERS-1 and Seasat scatterometers. Proc Int Geosci Remote Sens Symp IGARSS '94, August 8–12, Pasadena, California, pp 2382–2384

Ebert EE, Curry JA (1993) An intermediate one-dimensional thermodynamic sea ice model for investigating ice-atmosphere interactions. J Geophys Res 98, no C6: 10085–10109

Hallikainen M, Winebrenner DP (1992) The physical basis for sea ice remote sensing. In: Carsey FD (ed) Microwave remote sensing of sea ice, 478, American Geophysical Union, Washington, DC

Jaynes ET (1982) On the rationale of maximum-entropy methods. Proc IEEE 70, no 9: 939–952

Livingstone CE, Onstott RG, Arsenault LD, Gray AL, Singh KP (1987) Microwave sea ice signatures near the onset of melt. IEEE Trans Geosci Remote Sens 25, no 2: 159–173

Long DG, Drinkwater MR (1994) Greenland ice-sheet surface properties observed by the Seasat-A scatterometer at enhanced resolution. J Glaciol 40, no 135: 213–230

Long DG, Hardin PJ, Whiting PT (1993) Resolution enhancement of spaceborne scatterometer data. IEEE Trans Geosci Remote Sens 31, no 3: 700–715

Long DG, Early DS, Drinkwater MR (1994) Enhanced resolution ERS-1 scatterometer imaging of southern hemisphere polar ice. Proc Int Geosci Remote Sens Symp IGARSS '94, August 8–12, Pasadena, California, pp 156–158

Maykut G, Untersteiner N (1971) Some results from a time dependent thermodynamic model of sea ice. J Geophys Res 76: 1550–1575

Onstott RG (1992) SAR and scatterometer signatures of sea ice. In: Carsey FD (ed) Microwave remote sensing of sea ice, 478, American Geophysical Union, Washington, DC

Onstott RG, Grenfell TC, Mätzler C, Luther CA, Svendsen EA (1987) Evolution of microwave sea ice signatures during early summer and midsummer in the marginal ice zone. J Geophys Res 92, no C7: 6825–6835

Parkinson C (1992) Spatial patterns of increases and decreases in the length of the sea ice season in the north polar region 1979–1986. J Geophys Res 97, no C9: 14377–14388

Percival DB, Walden AT (1993) Spectral analysis for physical applications. Cambridge University Press, Cambridge, UK

Scharfen G, Barry RG, Robinson DA, Kukla G, Serreze MC (1987) Large-scale patterns of snow melt on Arctic sea ice mapped from meteorological satellite imagery. Ann Glaciol 9: 200–205

Schwartz K, Jeffries MO, Li S (1994) Using ERS 1 SAR data to monitor the state of Arctic Ocean sea ice between spring and autumn 1992. Proc Int Geosci Remote Sens Symp IGARSS '94, August 8–12, Pasadena, California, pp 1759–1762

Smith LC, Forster RR, Isacks BL, Hall DK (1997) Seasonal climatic forcing of alpine glaciers revealed with orbital synthetic aperture radar. J. Glaciol, in press

Winebrenner DP, Nelson ED, Colony R, West RD (1994) Observation of melt onset on multiyear Arctic sea ice using the ERS 1 synthetic aperture radar. J Geophys Res 99, no C11: 22425–22441

Winebrenner DP, Holt B, Nelson ED (1996) Observation of autumn freeze-up in the Beaufort and Chukchi Seas using the ERS 1 synthetic aperture radar. J Geophys Res 101, no C7: 16401–16419

Wismann V, Cavanie A, Hoekman D, Woodhouse I, Boehnke K, Schmullius C (1996) Land surface observations using the ERS-1 windscatterometer. Final Report for European Space Agency Contract 11103/94/NL/CN, Institute for Applied Remote Sensing, Wedel, Germany